Preprint Title	Boosting of photocatalytic hydrogen evolution via chlorine doping of polymeric carbon nitride
Authors	Malgorzata Aleksandrzak, Michalina Kijaczko, Wojciech Kukulka, Daria Baranowska, Martyna Baca, Beata Zielinska and Ewa Mijowska
Publication Date	04 Feb. 2021
Article Type	Full Research Paper
ORCID® iDs	Malgorzata Aleksandrzak - https://orcid.org/0000-0001-8654-3388; Wojciech Kukulka - https://orcid.org/0000-0003-2709-8741; Daria Baranowska - https://orcid.org/0000-0003-1969-8552

Boosting of photocatalytic hydrogen evolution via chlorine doping of polymeric carbon nitride

Malgorzata Aleksandrzak*, Michalina Kijaczko, Wojciech Kukulka, Daria Baranowska, Martyna Baca, Beata Zielinska, Ewa Mijowska

Nanomaterials Physicochemistry Department, Faculty of Chemical Technology and Engineering, West Pomeranian University of Technology, Szczecin, Piastow Ave. 42, 71-065 Szczecin, Poland

*Corresponding author: mwojtoniszak@zut.edu.pl, +48 91 449 6031

Abstract

Chemical doping is an effective strategy for modifying the electrochemical properties of polymeric carbon nitride and tuning its visible-light photocatalytic activity. In this study, chlorine-doped polymeric carbon nitride (Cl-PCN) has been synthesized by the polycondensation method. Among a series of samples, 200Cl-PCN exhibited the best photocatalytic activities for the hydrogen evolution from water splitting. Main aspects were revealed: (i) unique location of Cl atoms at the interlayers of PCN instead of on its π-conjugated planes, (ii) slight band gap narrowing, (iii) lower recombination rate of the electron-hole pairs, and (iv) improved photogenerated charge transport and separation. The above factors affected the 4.4-fold enhancement of photocatalytic efficiency in hydrogen evolution in comparison to the pristine catalyst.

Keywords

polymeric carbon nitride, hydrogen, photocatalysis, doping, chlorine

Introduction

Currently, the biggest problems of civilization seem to be the global energy crisis and environmental pollution. Both of these problems are directly related to each other. Pollution of our planet is mainly due to fossil fuels used in energy industry, the combustion of which causes CO_2 emissions.

The ideal solution of these problems appears to be the use of photocatalysis. The solar light, as a driving force, has been widely used in the different fields, such as water splitting to generate hydrogen [1], [2], [3], [4], environmental remediation [5], [6] decomposition of organic pollutants [7], CO_2 reduction into hydrocarbon fuels [8], [9], [10], disinfection [11], [12] and selective organic transformations [13], [14].

One of the most studied catalysts is polymeric carbon nitride (PCN). This graphite-like semiconductor polymer, as a metal-free and visible light-responsive photocatalyst, has attracted dramatically growing attention in the field of visible-light-induced hydrogen evolution reaction (HER). It is characterized by facile synthesis, easy functionalization, attractive electronic band structure and photocatalytic activity [15], [16], [17]. Furthermore, it exhibits high thermal and chemical stability during photocatalytic reactions in aqueous phase [18]. Unfortunately, its catalytic performance is mainly constrained by several typical challenges, which are low density of reactive sites, nonresponse in the long wavelength region, sluggish kinetics and high recombination of photoexcited electron–hole pairs [19], [20], [21].

Tremendous efforts have been made in order to increase the photocatalytic activity by optimizing the nanostructure and improving the chemical surface texture of PCN materials. Three of the most popular modification are: (i) coupling with other semiconductors [22], [23], (ii) self-optimization of the crystal structure [24], [25] and (iii) doping with heteroatoms [26], [27]. Therefore, PCN is called the "holy grail" because it is believed that its modification will result in obtaining a highly efficient HER under visible light conditions [28], [29].

One of the most effective methods of modifying the electronic structure and improving photocatalytic properties, among so many options, seems to be non-metallic doping [30], [31]. For instance, Ma et al. found that the doping of PCN with the P atom may promote the mobility of the charge carrier and facilitate the separation of the photogenerated electron -holes [32]. Another research group found that their prepared fluorinated carbon nitride has a photocatalytic activity 20.8 times higher than that of pristine PCN [30]. Wang et al. studied photoactivity of PCN doped with S in CO_2 reduction reaction. The yield of CH_3OH over the unit area of the photocatalyst was almost 2.5 times higher than for the pristine PCN [33].

Recently, co-doping of g-C_3N_4 with two non-metallic elements has been also studied. This strategy can enhance photocatalysis by imparting additional merits of each co-dopants to the photocatalyst. Polymeric carbon nitride has been co-doped with B / F [34], S / P [35] or C / P [36]. Yi et al. showed that PCN co-doped with S and Cl had better catalytic efficiency in the degradation of rhodamine B and 4-nitrophenol in visible light compared to catalysts doped with one heteroatom [37]. Other studies showed that S and P doped photocatalyst showed

significantly increased photocatalytic activity in the degradation of methylene blue under visible light, compared to the bulk PCN. The improvement was attributed to lone electron delocalization, efficient charge separation, favorable retention of the crystal structure and light harvesting extension [38].

Here, a new procedure of PCN doping with chlorine will be revealed. The photocatalytic activity of the prepared materials was investigated in water splitting reaction with hydrogen evolution under simulated solar light. A series of microscopic and spectroscopic techniques has been used to characterize the morphology, chemical structure, optical, photophysical and electrical properties of the obtained carbon nitrides.

Experimental section

2.1. Materials

All reagents employed for catalyst preparation were purchased in analytical grade and used without further purification.

2.2. Synthesis of polymeric carbon nitride

Polymeric carbon nitride was synthesized by direct heating of melamine. A given amount of melamine was placed in a covered crucible in a muffle furnace and heated in static air to 550 °C with a ramping rate of 4 °C /min and then was held at 550 °C for 4 h. After the reaction, the furnace was cooled down to room temperature. The obtained PCN was collected and milled in an agate mortar into powder.

2.3. Synthesis of Cl-doped polymeric carbon nitride

As a precursor of chlorine 2-chloro-4,6-diamino-1,3,5-triazine (CDATA) was used. Firstly, melamine (4 g) was mixed with different amounts (100 mg/200 mg/400 mg) of CDATA in 20 mL deionized water with stirring for 1 h at room temperature. The solutions were then dried at 80 °C overnight. The obtained powders were ground in an agate mortar and placed in covered crucibles, followed by thermal condensation under the same conditions as the PCN. The final products were milled in a mortar into a fine powder. Synthesis conditions are listed in Table 1.

Table 1. Preparation conditions of Cl-doped polymeric carbon nitride.

Sample	Melamine [g]	CDATA [mg]	Temperature [°C]	Heating rate [°C/min]	Time [h]
PCN	10	-	550	4	4
100Cl-PCN	4	100	550	4	4
200Cl-PCN	4	200	550	4	4
400Cl-PCN	4	400	550	4	4

2.4. Characterization

Morphology of the samples was analyzed using transmission electron microscopy (TEM, Tecnai F30) with 200 kV accelerating voltage. Fourier transform infrared (FTIR) spectra were recorded on Nicolet 6700 FT-IR Spectrometer. The chemical composition and relative atomic percentages on the surface of the samples were studied by X-ray Photoelectron Spectroscopy (XPS). The measurements were conducted using Mg Ka (hν = 1253.6 eV) radiation in a Prevac (Poland) system equipped with a Scienta SES 2002 (Sweden) electron energy analyzer operating with constant transmission energy (Ep = 50 eV). The analysis chamber was evacuated to a pressure below $5 \cdot 10^{-9}$ mbar. The photoluminescence (PL) spectra were measured using fluorescence spectrophotometer F7000 (Hitachi) with excitation wavelength of 280 nm. The UV–vis diffuse reflectance spectra (DRS) were performed using a Jasco (Japan) spectrometer. Kubelka-Munk function was used to calculate the band gap energy. Photocurrent response and electrochemical impedance spectroscopy (EIS) were measured on Autolab PGSTAT302 N potentiostat. Details of the procedure are presented elsewhere [39].

2.5. Photocatalytic test

Prior to the photocatalytic test, each sample was prepared by dispersing 10 mg of the photocatalyst in 20 ml of water and sonicated for 1 hour. The photocatalytic water splitting reaction was carried out in an outer irradiation-type reactor (Pyrex reaction vessel) connected to argon. After the reaction solution was placed in the reactor, 5 mL of lactic acid was poured to and purged with argon to remove air. Then, the reactor was irradiated with Xe lamp (150 W) with air mass filter (A.M. 1.5 G) to achieve a simulated solar light. The photocatalytic H_2 evolution rate was analyzed by Young Lin 6500 gas chromatograph (GC, Micro TCD detector, ValcoPLOT Molesieve 5 Å Fused Silica Column and Ar as a carrier). Each catalyst was tested for 3 hours. Every hour, 100 µL of gas was withdrawn from the reactor and injected into the gas chromatograph to measure the amount of H_2 evolved.

Results and discussion

The detailed analysis of the morphology of the prepared materials, presented in Fig. 1, was performed with transmission electron microscopy (TEM). The images of pristine PCN demonstrate the layered structure with tendency to fold and aggregate. It also shows several stacking layers, indicating the planar graphitic-like structure. After Cl-doping, relatively uniform stacked petal-like nanosheets structure with small pores on the surface was formed (Fig. 1). Deep magnification shows that in-plane mesopores of tens of nanometers are randomly distributed on the carbon nitride nanosheets (Figure 1c). The 200Cl-PCN porous structure allows the catalyst to produce a higher specific surface area and more active sites, which can simultaneously promote mass transfer and charge separation in nanodomains, thus optimizing the π-conjugated system for photochemical applications [40], [41].

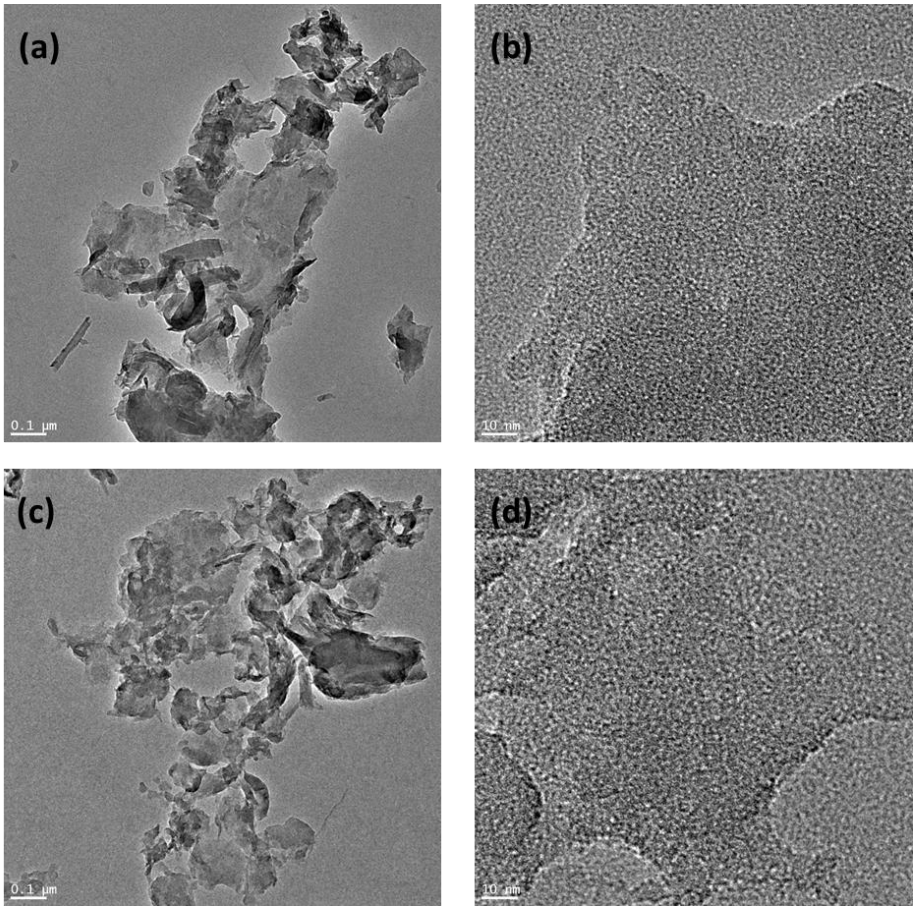

Figure 1. TEM images of PCN (a, b) and 200Cl-PCN (c, d).

As analyzed via AFM (Fig. 2a-b) the as-prepared PCN aggregated as large sheets with thickness from 1 to 4 nm (corresponding to 3-11 atomic layers). In comparison, the Cl-doped PCN (2c-d) revealed the thickness from 0.5 to 5 nm (giving 2-14 atomic layers) with the peak

located at 2-4 nm. Slight enlargement of lattice parameters might be explained by unique location of Cl atoms at the interlayers of PCN and not on its π-conjugated planes as it is in the case with other common use metals/non-metals (Cu, Ni, C, N or O) modifications [42-46].

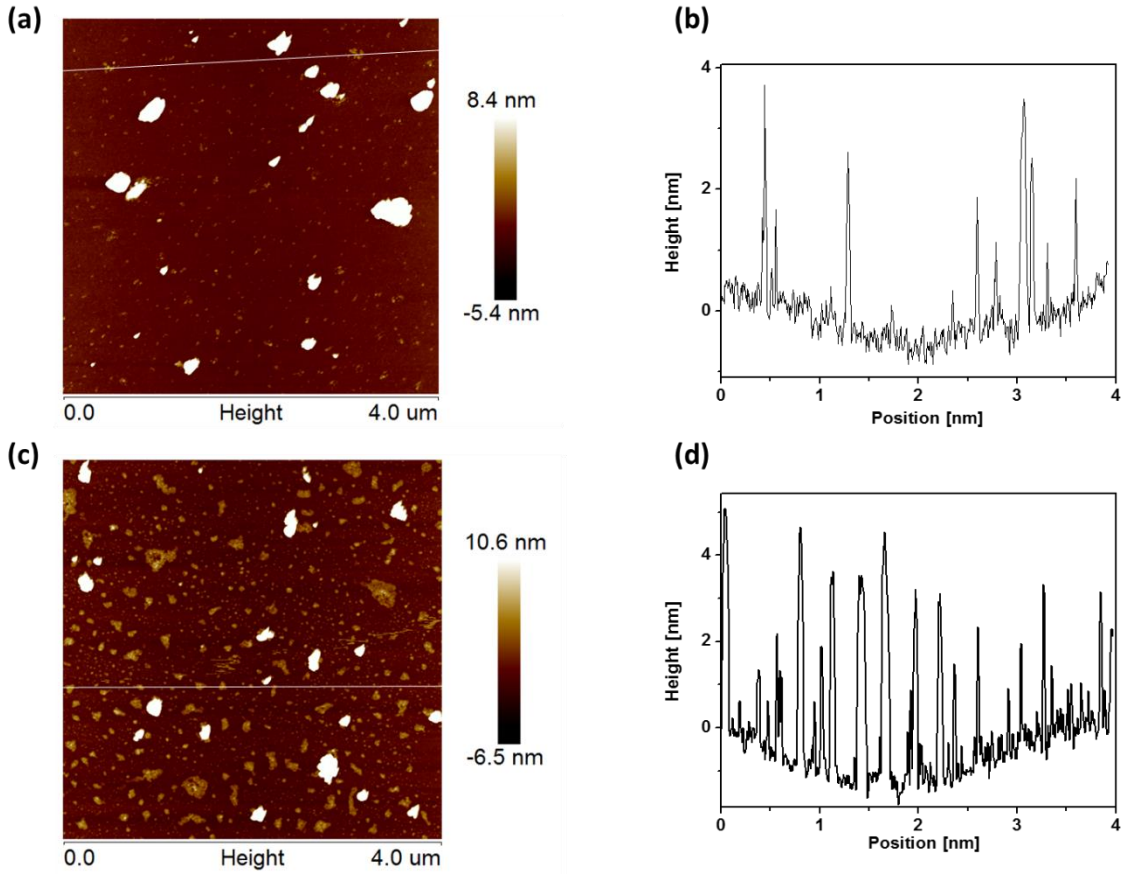

Figure 2. AFM images and height profile of PCN (a, b) and 200Cl-PCN (c, d).

Fourier Transform Infrared (FTIR) Spectroscopy was used to illustrate the molecular structure information on the carbon nitride materials. FTIR absorption analysis was recorded in the spectral range of 600 – 3600 cm^{-1} to examine the surface of the prepared materials (Fig. 3a). FTIR spectra of both samples (before and after doping) reveal nearly the same positions of the vibration peaks, indicating similar molecular structure of the samples which is well maintained even after chemical doping of Cl. The signal at 810 cm^{-1} represents the s-triazine ring models, which corresponds to the condensed CN heterocycles. The intense signal between 1200 and 1600 cm^{-1} are indicative of the characteristic stretching vibration of CN heterocycles [47], [48], [49]. To be more specific, the peaks at 1241, 1318, and 1425 cm^{-1} are assigned to the aromatic C–N stretching [50], [51] while 1572 and 1637 cm^{-1} correspond to C=N stretching [52]. The broad peaks in the range of 3000–3600 cm^{-1} correspond to uncondensed terminal

amino groups (-NH_2 or = NH) [53], [54]. The spectra do not show Cl-contained functional groups, which can be attributed to its relative low amount and the signal may be overlapped by CN vibration.

The XRD (Fig. 3b) showed that both samples displayed similar crystalline phase with two characteristic peaks at about 27.38˚ and 13.28˚, corresponding to (002) and (100) crystal planes for PCN. The (002) peak is associated with the typical interplanar stacking peak of conjugated aromatic structure, whereas the (100) peak is attributed to in-plane packing motif of tri-s-triazine units. The shift from 27.38˚ to 27.30˚ is caused by increased internal distance of PCN by Cl doping, which is in good agreement with AFM data. Moreover, the XRD and FTIR analysis confirmed that Cl-modification resulted in maintenance the chemical skeleton [42-46].

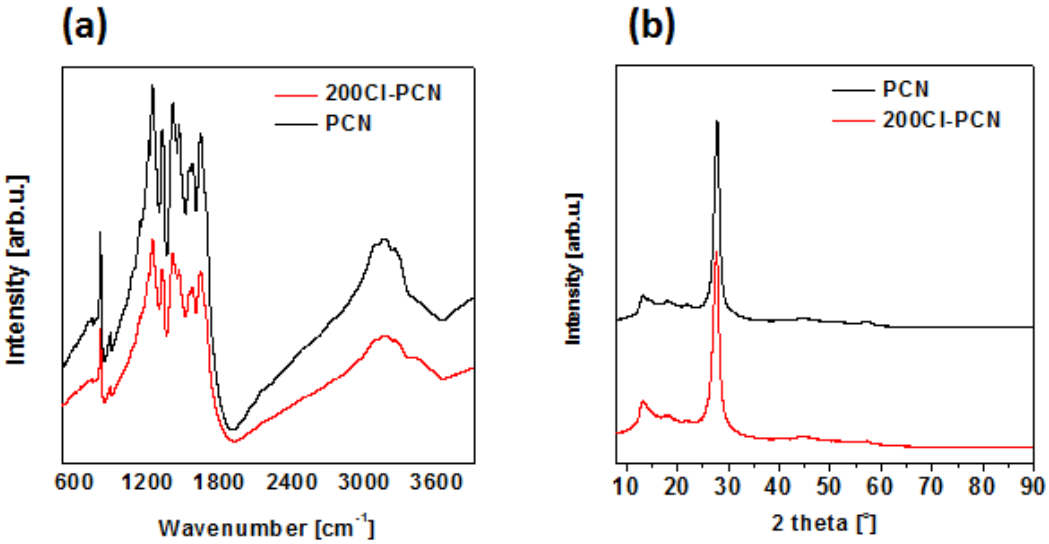

Figure 3. (a) FTIR spectra and (b) XRD patterns of PCN and 200Cl-PCN.

The chemical composition and relative atomic percentages of the obtained materials were analyzed by XPS measurements. The XPS spectra revealed the samples are composed of carbon, nitrogen and oxygen. Additionally, chlorine signal detected in the doped samples. The atomic concentration of the elements has been calculated assuming homogeneous distribution in the analyzed surface layer and is given in Table 2. The obtained results show that the content of nitrogen, carbon and oxygen is similar for all three samples. In the case of chlorine, no signal can be observed for the initial sample (PCN). For the sample 100Cl-PCN, a small amount of chlorine appears (0.04 at.%) which increases even more for the sample 200Cl-PCN (0.18 at.%). The detailed analysis of the chemical components of carbon and nitrogen has been done by peak fitting procedure applied to the N1s and C1s spectra of the obtained samples. The results

of that analysis are shown in Fig. 4 and in Table 3. The type of the binding energy as well as the relative contribution of each component to the total area under the peak were calculated. The spectra of both N 1s and C 1s of PCN present the typical shapes as well as the peak positions (~399 and ~288 eV for N 1s and C 1s, respectively). The N 1s spectra present three main contributions, related to C–N_3 (N_3C), N–C=N (N_2C), and N–H_x contributions, while the C 1s region shows three contributions assigned to C–C, N–C=N and C–NH_x. The sample 200Cl-PCN presents additional contribution at 289 eV, related to C-Cl. It can be observed that as a result of chlorine functionalization the share of N-H_x/C-NH_x components increases compared to the starting material. In the case of the 200Cl-PCN, the content of N-C=N/N_2C bonds is also increasing. On the other hand, the content of C-C/C=C/N_3C is significantly decreasing.

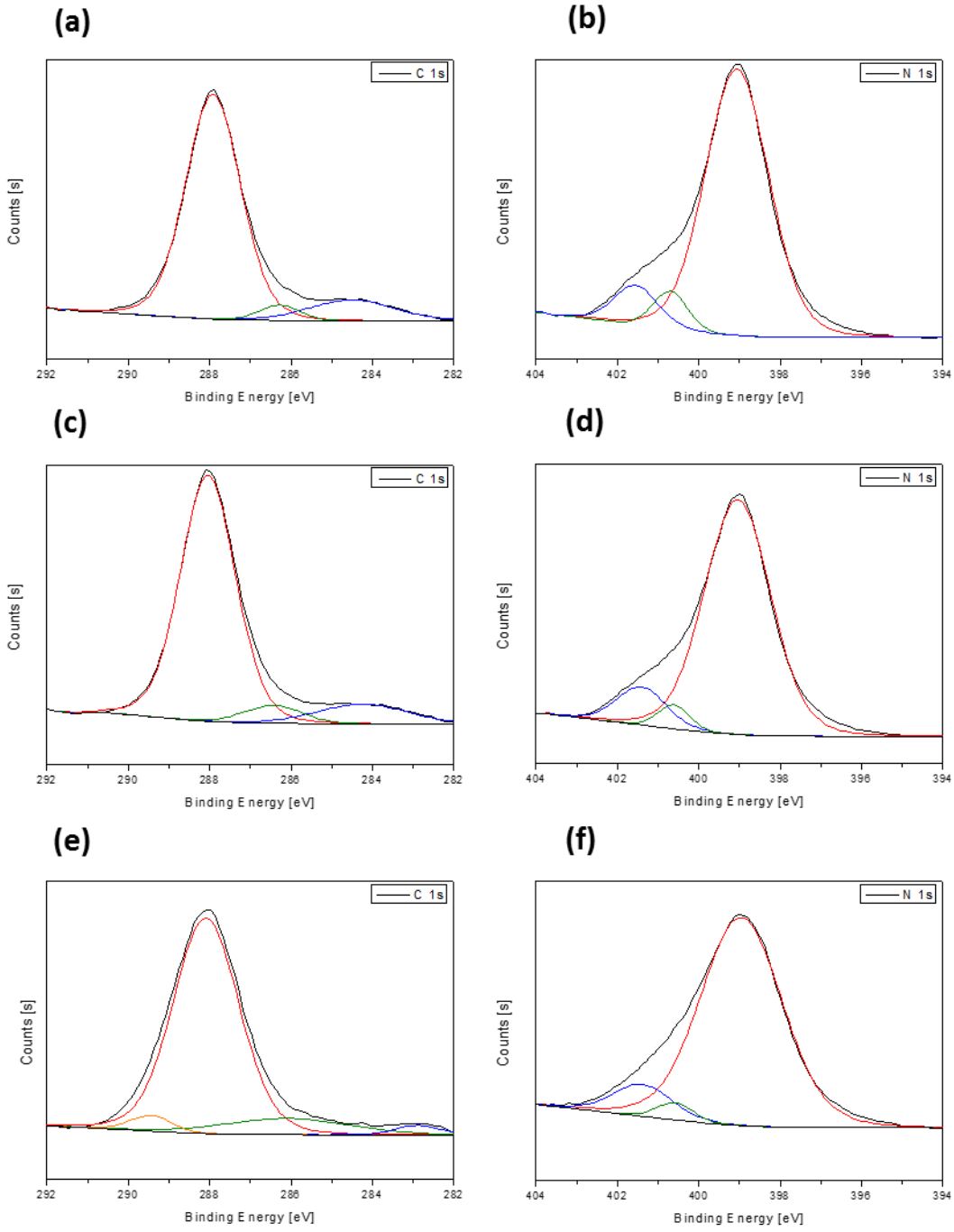

Figure 4. C 1s and N 1s XPS spectra of polymeric carbon nitride (a, b), 100Cl-PCN (c, d) and 200Cl-PCN (e, f).

The XPS analysis indicates successful incorporation of chlorine into the polymeric carbon nitride network. Without doping agent melamine thermal polycondensation leads to formation of melon. We suppose that the presented synthesis procedure results in substitution of melamine molecule with 2-chloro-4,6-diamino-1,3,5-triazine to form Cl-doped melon, followed by further polycondensation leading to chlorine-doped polymeric carbon nitride. The

substitution had an effect on appearance of C-Cl bonding in the PCN structure. Moreover, it resulted in decrease in the amount of C-NH_x bonding from 4.23 % to 2.49 %, decrease in N_3-C contribution from 6.50 % to 3.23 % and simultaneously, increase in N_2-C binding from 84.77 % to 87.23 %, when PCN is compared to 200Cl-PCN, respectively. Schematic representation of the as—synthesized material structure is presented in Figure 5.

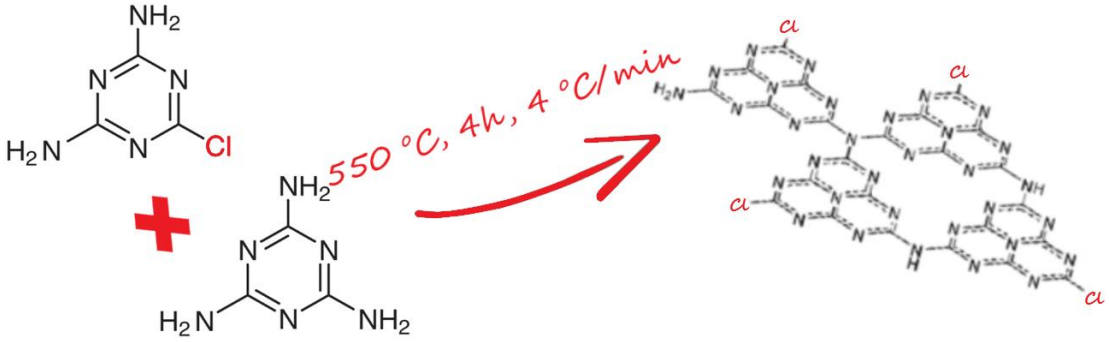

Figure 5. Structure of chlorine-doped polymeric carbon nitride.

Table 2. C, N, O and Cl atomic concentration of PCN, 100Cl-PCN and 200Cl-PCN.

Sample	C (at.%)	N (at.%)	O (at.%)	Cl (at.%)
PCN	36	63.58	0.42	-
100Cl-PCN	34.65	64.96	0.35	0.04
200Cl-PCN	36.86	62.31	0.65	0.18

Table 3. Chemical composition of PCN, 100Cl-PCN and 200Cl-PCN calculated from peak fitting procedure applied to the N 1s and C 1s spectra of the samples.

Sample	N-C=N (at.%)	C-NH_x (at.%)	C-C/C=C (at.%)	C-Cl (at.%)	N_2C (at.%)	N-H_x (at.%)	N_3C (at.%)
PCN	83.61	4.23	12.16	-	84.77	8.73	6.50
100Cl-PCN	82.91	6.19	10.90	-	85.64	10.28	4.08
200Cl-PCN	82.13	2.49	11.67	3.71	87.23	9.54	3.23

The porosity of polymeric carbon nitride and PCN doped with chlorine was tested by the N_2 adsorption–desorption experiment. The typical IV isotherms with H3 hysteresis loops are observed in the samples, which is typical of mesoporous materials (Fig. 6). The hysteresis loops, pore size distribution curves and average pore diameter for both samples are similar. The proportion of micropores is small and the samples contain mainly mesopores. The sample modified by chlorine presents slightly higher BET surface area and average pore diameter but lower total pore volume.

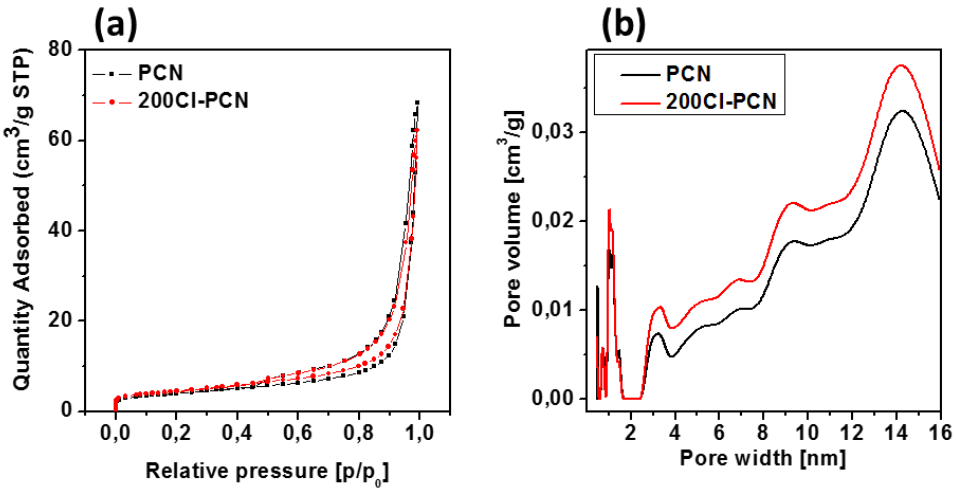

Figure 6. (a) Adsorption-desorption isotherms and (b) DFT adsorption pore size distribution of polymeric carbon nitride and PCN doped with Cl.

Table 4. BET surface area, T-plot micropore area, external surface area, total pore volume and average pore diameter of PCN and 200Cl-PCN.

Sample	PCN	200Cl-PCN
BET surface area [m²/g]	14,43 ± 0,02	16,27 ± 0,01
T- plot micropore area [m²/g]	2,06	1,94
T-plot external surface area [m²/g]	12,37	14,32
Total pore volume [cm³/g]	0,106	0,096
Average pore diameter [nm]	5,65	5,76

The results of photocatalytic hydrogen generation process under simulated solar light irradiation is presented in Fig. 7. It is clear that the designed modification of the samples strongly boosts the photocatalytic efficiency. Hydrogen evolution of 100Cl-PCN was about

3.3- times higher after 3h. Simultaneously, 200Cl-PCN produced approximately 4.4- times more hydrogen in relation to unmodified PCN. Therefore, chlorine doping is reasonable strategy towards better photocatalytic hydrogen generation ability. However, this effect is not observed in 400Cl-PCN what proves that optimalization of the operational conditions is crucial.

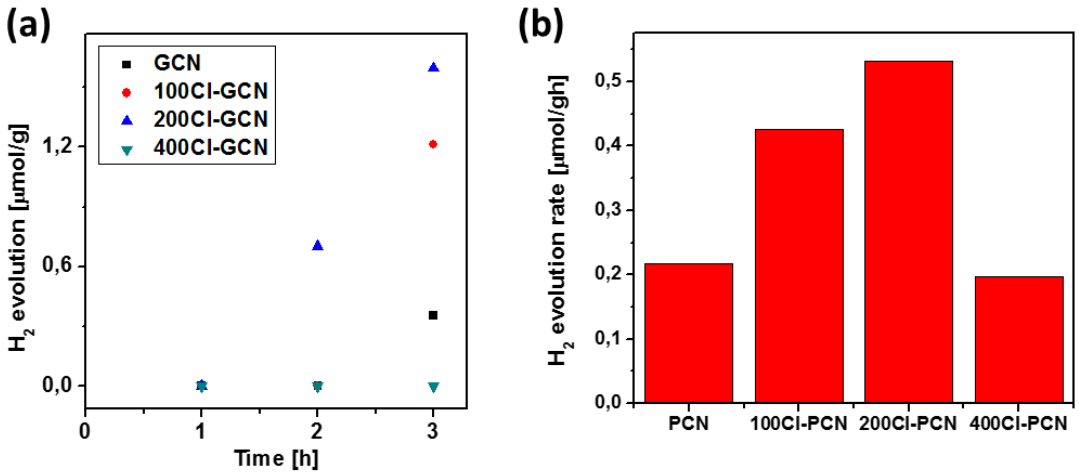

Figure 7. H_2 evolution rate catalyzed by PCN, 100Cl-PCN, 200Cl-PCN and 400Cl-PCN.

To explain the phenomenon of the most efficient photocatalyst (200Cl-PCN) more studies have been conducted. The optical properties of PCN and 200Cl-PCN were investigated through UV-vis diffuse reflectance spectra (DRS) and photoluminescence (PL) emission spectra. Fig. 8(a) shows the Kubelka-Munk function curves of the fabricated materials. The band gap is 2.78, and 2.77 eV for PCN and 200Cl-PCN, respectively, indicating that Cl-doping had not a significant effect on the band gap shift. This might be attributed to the low content of chlorine atoms in the material.

Next, PL spectra of PCN and 200Cl-PCN are recorded as illustrated in Fig. 8(b). The emission peak of PCN is located at about 440 nm under excitation at 640 nm. While the emission peak is red-shifted slightly in the case of 200Cl-PCN. The red shift of emission peak is in good agreement with DRS measurement. Additionally, it can be found that the peak intensity of 200Cl-PCN is lower than that of PCN, reflecting a lower recombination rate of the electron-hole pairs, which is desirable in the photocatalytic process. That shows that Cl doping can significantly promote the visible light absorption and improve the utilization of visible light of PCN, which promote the photocatalytic activity [47].

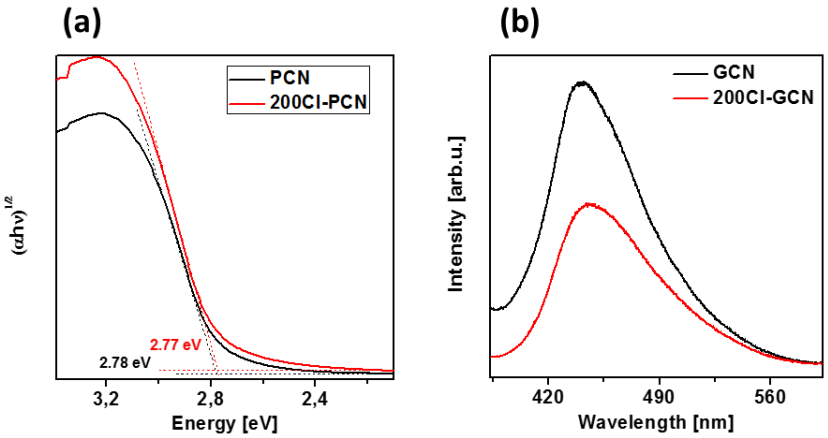

Figure 8. DRS (a) and PL emission (b) spectra of PCN and 200Cl-PCN.

Figure 9(a) shows the transient photocurrent response *(I-t)* of PCN and 200Cl-PCN. The photocurrent of 200Cl-PCN is about 2 times higher than that of PCN, indicating that Cl-doped PCN can generate more photoelectrons and the photogenerated electron-hole pairs are separated more effectively. After 3 cycles of light on-off, the performance of both electrodes tends to stabilize, indicating that the photocatalysts are stable under visible light irradiation.

Electrochemical impedance spectroscopy (EIS) is shown in Fig. 9(b). It is known that the arc radius of the EIS spectrum is related to the charge transfer resistance at the electrode-electrolyte interface [48]. The EIS arc radius of 200Cl-PCN is smaller than that of PCN, and its impedance is reduced compared to PCN, indicating that Cl doping decreased the charge transfer resistance of polymeric carbon nitride. It further indicates that Cl doping can promote photogenerated carriers transfer and separation [47], which is in agreement with photoluminescent spectroscopy.

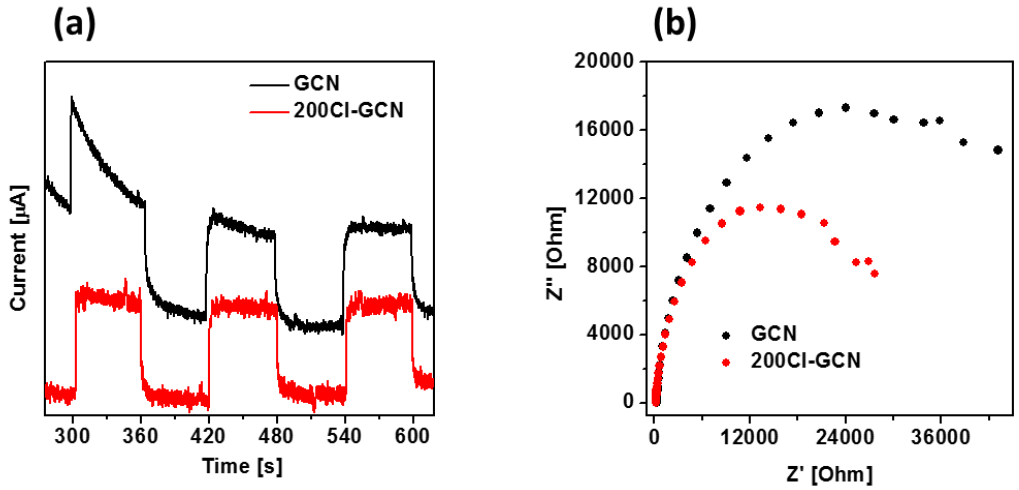

Figure 9. Photocurrent response (a) and EIS spectra (b) of PCN and 200Cl-PCN.

The presented study revealed that polycondensation of melamine with 2-chloro-4,6-diamino-1,3,5-triazine leads to formation of Cl-doped polymeric carbon nitride. The presented material showed the improved photocatalytic properties in hydrogen evolution reaction from water compared to pristine PCN. The investigation showed that the enhanced photocatalytic activity was attributed to the improved photogenerated charge transport and separation. Although Cl doping did not affect reduction in band gap energy, the transient photocurrent response of 200Cl-PCN was enhanced compared to pristine PCN indicating better transport and separation of the photoinduced charges. It indicates that higher amount of electrons can migrate to the surface reaction sites before recombination leading to hydrogen evolution. These results are in consistence with PL spectroscopy and EIS spectroscopy, revealing the better separation and charge transfer, respectively, after chlorine doping.

Conclusions

In summary, Cl-PCN nanosheets have been successfully synthesized by the polycondensation method. Fabricated 2D nanomaterials were used as photocatalysts for hydrogen evolution from water splitting. The optimization of chlorine was also performed. It was found that Cl-modification had an effect on photocatalytic efficiency. Also, main aspects were revealed: (i) unique location of Cl atoms at the interlayers of PCN and not on its π-conjugated planes, (ii) not the reduction in the band gap, (iii) the lower recombination rate of the electron-hole pairs, and (iv) improved photogenerated charge transport and separation. Therefore, it is believed that heteroatom doping of pristine PCN is a suitable strategy towards boosting photocatalytic hydrogen evolution.

Acknowledgements

This work was financially supported by the National Science Center, Poland, under SONATA program (no. 2015/19/D/ST5/01920).

References

[1] A. Kudo, Y. Miseki, Heterogeneous photocatalyst materials for water splitting, Chem. Soc. Rev., 38 (2009), p. 253

[2] T. Hisatomi, K. Domen, Reaction systems for solar hydrogen production via water splitting with particulate semiconductor photocatalysts, Nature Catalysis 2 (2019), p. 387–399

[3] X. Chen, S. Shen, L. Guo, S. S. Mao, Semiconductor-based Photocatalytic Hydrogen Generation, Chem. Rev. (2010), p. 6503–6570

[4] K. Maeda, Z-Scheme Water Splitting Using Two Different Semiconductor Photocatalysts, ACS Catalysis (2013), p. 1486–1503

[5] H. Zhang, G. Chen, D. W. Bahnemann, Photoelectrocatalytic materials for environmental applications, Journal of Materials Chemistry, 27 (2009), p. 5089-5121

[6] A. Di Paola, E. García-López, G. Marcì, L. Palmisano, A survey of photocatalytic materials for environmental remediation, Journal of Hazardous Materials (2012), p. 3-29

[7] D. Chatterjee, S. Dasgupta, Visible light induced photocatalytic degradation of organic pollutants, J. Photochem. Photobiol. C., 6 (2005), p. 186

[8] M. Marszewski, S. Cao, J. Yu, M. Jaroniec, Semiconductor-based photocatalytic CO2 conversion, Materials Horizons, 3 (2015), p. 261-278

[9] J. Yu, K. Wang, W. Xiao, B. Chenga, Photocatalytic reduction of CO2 into hydrocarbon solar fuels over g-C3N4–Pt nanocomposite photocatalysts, Physical Chemistry Chemical Physics, 23 (2014)

[10] S. Yu, P. K. Jain, Selective Branching of Plasmonic Photosynthesis into Hydrocarbon Production and Hydrogen Generation, ACS Energy Lett., 9 (2019), p. 2295–2300

[11] S. Malato, P. Fernández-Ibáñez, M. Maldonado, J. Blanco, W. Gernjak, Decontamination and disinfection of water by solar photocatalysis: Recent overview and trends, Catalysis, 1 (2009), p. 1-59

[12] P.K. Robertson, J.M. Robertson, D.W. Bahnemann, Removal of microorganisms and their chemical metabolites from water using semiconductor photocatalysis, J. Hazard. Mater., 161 (2012), p. 211-212

[13] Y. Shiraishi, T. Hirai, ,Selective organic transformations on titanium oxide-based photocatalysts, Journal of Photochemistry and Photobiology C: Photochemistry Reviews, 4 (2008), p. 157-170

[14] X. Lang, X. Chen, J. Zhao, Heterogeneous visible light photocatalysis for selective organic transformations, Chemical Society Reviews, 1 (2014), p. 473-486

[15] P. Niu, L. Zhang, G. Liu, H. M. Cheng, Graphene-Like Carbon Nitride Nanosheets for Improved Photocatalytic Activities, Adv. Funct. Mater., 22 (2012), p. 4763-4770

[16] Y. Zheng, L. H. Lin, B. Wang, X. C. Wang, Graphitic Carbon Nitride Polymers toward Sustainable Photoredox Catalysis, Angew. Chem., Int. Ed., 44 (2015), p. 12868-12884

[17] K. R. Reddy, C. H. V. Reddy, M. N. Nadagoudac, N. P. Shettid, S. Jaesoolb, T. M. Aminabhavi, Polymeric Graphitic Carbon Nitride (g-C3N4)-Based Semiconducting Nanostructured Materials: Synthesis Methods, Properties and Photocatalytic Applications, J. Environ. Manage. (2019), p. 25-40

[18] W.-J. Ong, L.-L. Tan, Y.H. Ng, S.-T. Yong, S.-P. Chai, Graphitic carbon nitride (g-C3N4)-based photocatalysts for artificial photosynthesis and environmental remediation: are we a step closer to achieving sustainability?, Chem. Rev., 12 (2016), p. 7159–7329

[19] J. Zhang, J. Sun, K. Maeda, K. Domen, P. Liu, M. Antonietti, X. Fu, X. Wang, Sulfurmediated synthesis of carbon nitride: Band-gap engineering and improved functions for photocatalysis, Energy Environ. Sci., 4 (2011), p. 675– 678

[20] G. Tan, L. She, T. Liu, X. Chi, H. Ren, X. Ao, Ultrasonic Chemical Synthesis of Hybrid Mpg-C3N4/BiPO4 Heterostructured Photocatalysts with Improved Visible Light Photocatalytic Activity, Appl. Catal. B: Environ. (2017), p. 120– 133,

[21] Y. Wang, X. C. Wang, M. Antonietti, Polymeric Graphitic Carbon Nitride as a Heterogeneous Organocatalyst: From Photochemistry to Multipurpose Catalysis to Sustainable Chemistry Angew Chem Int Ed Engl, 1 (2012), p. 68-89

[22] W. L. Yu, D. F. Xu, T. Y. Peng, Enhanced photocatalytic activity of g-C3N4 for selective CO2 reduction to CH3OH via facile coupling of ZnO: a direct Z-scheme mechanism, J. Mater. Chem. A, 39 (2015), p. 19936-19947

[23] S. Zhou, Y. Liu, J. Li, Y. Wang, G. Jiang, Z. Zhao, D. Wang, A. Duan, J. Liu, Y. Wei, Facile in situ synthesis of graphitic carbon nitride (g-C3N4)-N-TiO2 heterojunction as an

efficient photocatalyst for the selective photoreduction of CO2 to CO, Appl. Catal., B, (2014), p. 20-29

[24] L. Wang, Y. Hong, E. Liu, Z. Wang, J. Chen, S. Yang, J. Wang, X. Lin, J. Shia, Rapid polymerization synthesizing high-crystalline g-C3N4 towards boosting solar photocatalytic H2 generation, International Journal of Hydrogen Energy, 11 (2020), p. 6425-6436

[25] Y. Kang, Y. Yang, L. C. Yin, X. Kang, G. Liu, H. M. Cheng, An Amorphous Carbon Nitride Photocatalyst with Greatly Extended Visible-Light-Responsive Range for Photocatalytic Hydrogen Generation, Adv. Mater., 13 (2015), p. 4572-4577

[26] S. C. Yan, Z. S. Li, Z. G. Zou, Photodegradation of Rhodamine B and Methyl Orange over Boron-Doped g-C3N4 under Visible Light Irradiation, Langmuir, 6 (2010), p. 3894–3901

[27] Z. A. Lan, G. G. Zhang, X. C. Wang, A facile synthesis of Br-modified g-C3N4 semiconductors for photoredox water splitting, Appl. Catal., B (2016), p. 116-125

[28] G. Liao, Y. Gong, L. Zhang, H. Gao, G. J. Yang, B.Fang, Semiconductor polymeric graphitic carbon nitride photocatalysts: the “holy grail” for photocatalytic hydrogen evolution reaction under visible light, Energy & Environmental Science, 7 (2019)

[29] N. L. Reddy, V. S.Kumbhar, K. Lee, M.V.Shankar, Chapter 9 - Graphitic carbon nitride–based nanocomposite materials for photocatalytic hydrogen generation, Nanostructured, Functional, and Flexible Materials for Energy Conversion and Storage Systems (2020), p. 293-324

[30] Y. Wang, Y. Di, M. Antonietti, H. Li, X. Chen, X. Wang, Excellent visible-light photocatalysis of fluorinated polymeric carbon nitride solids, Chemistry of Materials, 18 (2010), p. 5119-5121

[31] J. Hong, D. K. Hwang, R. Selvaraj, Y. Kima, Facile synthesis of Br-doped g-C3N4 nanosheets via one-step exfoliation using ammonium bromide for photodegradation of oxytetracycline antibiotics, Journal of Industrial and Engineering Chemistry (2019), p. 473-481

[32] X. Ma, Y. Lv, J. Xu, Y. Liu, R. Zhang, Y. Zhu, A strategy of enhancing the photoactivity of g-C3N4 via doping of nonmetal elements: a first-principles study, J. Phys. Chem. C, 116 (2012), p. 23485-23493

[33] Y. Wang, Y. Di, M. Antonietti, H. R. Li, X. F. Chen, X. C. Wang, Excellent visible-light photocatalysis of fluorinated polymeric carbon nitride solids, Chem. Mater., 22 (2010), p. 5119-5121

[34] K. Wang, Q. Li, B. Liu, B. Cheng, W. Ho, J. Yu, Sulfur-doped g-C3N4 with enhanced photocatalytic CO2-reduction performance, Applied Catalysis B: Environmental (2015), p. 44-52

[35] K. N. Ding, L. L. Wen, M. Y. Huang, Y. F. Zhang, Y. P. Lu, Z. F. Chen, How does the B, F-monodoping and B/F-codoping affect the photocatalytic water-splitting performance of g-C3N4?, Phys. Chem. Chem. Phys., 28 (2016), p. 19217-19226

[36] C. C. Hu, W. Z. Hung, M. S. Wang, P. J. Lu, Phosphorus and sulfur codoped g-C3N4 as an efficient metal-free photocatalyst, Carbon, 127 (2018), p. 374-383

[37] H. Wang, B. Wang, Y. R. Bian, L. M. Dai, Enhancing photocatalytic activity of graphitic carbon nitride by codoping with P and C for efficient hydrogen generation, ACS Appl. Mater. Inter., 26 (2017), p. 21730-21737

[38] F. Yi, H. Gan, H. Jin, W. Zhao, K. Zhang, H. Jin, H. Zhang, Y. Qian, J. Ma, Sulfur- and chlorine-co-doped g-C3N4 nanosheets with enhanced active species generation for boosting visible-light photodegradation activity, Separation and Purification Technology (2020)

[39] C. C. Hu, W. Z. Hung, M. S. Wang, P. J. Lu, Phosphorus and sulfur codoped g-C3N4 as an efficient metal-free photocatalyst, Carbon, 127 (2018), p. 374-383

[40] J. Liu, J. Huang, H. Zhou, M Antonietti, Uniform Graphitic Carbon Nitride Nanorod for Efficient Photocatalytic Hydrogen Evolution and Sustained Photoenzymatic Catalysis, ACS Appl. Mater. Interfaces, 6 (2014), p. 8434– 8440

[41] S. Chen, J. Duan, Y. Tang, S. Z. Qiao, Hybrid Hydrogels of Porous Graphene and Nickel Hydroxide as Advanced Supercapacitor Materials, Chem. - Eur. J.,19 (2013), p. 7118– 7124

[42] Zhao, Daming, et al. "Interlayer interaction in ultrathin nanosheets of graphitic carbon nitride for efficient photocatalytic hydrogen evolution." *Journal of catalysis* 352 (2017): 491-497.

[43] Wang, Nan, et al. "Fluorine-doped carbon nitride quantum dots: Ethylene glycol-assisted synthesis, fluorescent properties, and their application for bacterial imaging." *Carbon* 109 (2016): 141-148.

[44] Han, Er-Xun, et al. "Chlorine doped graphitic carbon nitride nanorings as an efficient photoresponsive catalyst for water oxidation and organic decomposition." *Journal of Materials Science & Technology* 35.10 (2019): 2288-2296.

[45] Liu, Chengyin, et al. "Chlorine intercalation in graphitic carbon nitride for efficient photocatalysis." *Applied Catalysis B: Environmental* 203 (2017): 465-474.

[46] Baca, M., et al. "Surface properties tuning of exfoliated graphitic carbon nitride for multiple photocatalytic performance." *Solar Energy* 207 (2020): 528-538.

[47] D. Long, W. Diao, X. Rao, Y. Zhang, Boosting the Photocatalytic Hydrogen Evolution Performance of Mg- and Cl-Doped Graphitic Carbon Nitride Microtubes, ACS Appl. Energy Mater. 2020, 3, 9, 9278–9284.

[48] Bu, Y.; Chen, Z.; Li, W. Using electrochemical methods to study the promotion mechanism of the photoelectric conversion performance of Ag-modified mesoporous g-C3N4 heterojunction material. Appl. Catal., B 2014, 144, 622−630.